Quasielastic scattering of ^{8}B and ^{7}Be on ^{12}C at 40 MeV/nucleon

I. Pecina,[1,2] R. Anne,[1] D. Bazin,[1] C. Borcea,[3] V. Borrel,[4] F. Carstoiu,[3] J. M. Corre,[1] Z. Dlouhy,[2] A. Fomitchev,[5] D. Guillemaud-Mueller,[4] H. Keller,[4] A. Kordyasz,[6] M. Lewitowicz,[1] S. Lukyanov,[1,5] A. C. Mueller,[4] Yu. Penionzhkevich,[5] P. Roussel-Chomaz,[1] M. G. Saint-Laurent,[1] N. Skobelev,[5] O. Sorlin,[4] and O. Tarasov[1,5]

[1] *Grand Accelerateur National d'Ions Lourds, Boîte Postale 5027, 14021 Caen Cedex, France*

[2] *Nuclear Physics Institute, 250 68 Rez, Czech Republic*

[3] *Institute of Atomic Physics, P.O. Box MG6, 76900 Bucharest-Magurele, Romania*

[4] *Institut de Physique Nucléaire, CNRS-Institut National de Physique Nucléaire et de Physique des Particules, 91406 Orsay Cedex, France*

[5] *Flerov Laboratory of Nuclear Reactions, Joint Institute for Nuclear Research, 141980 Dubna, Moscow Region, Russia*

[6] *Institute of Experimental Physics, Warsaw University, Hoża 69, 00681 Warsaw, Poland*

(Received 6 September 1994)

The quasielastic scattering of the exotic nucleus ^{8}B on a ^{12}C target has been studied at an energy of 320 MeV and compared with that of ^{7}Be at the same velocity. The quasielastic scattering of ^{12}C+^{12}C at 20 MeV/nucleon, also performed as a secondary beam experiment, was used to check the data reduction method. The results are interpreted in terms of a semimicroscopic double folding model and coupled-channels calculation. The difference in the total reaction cross section (8%) between ^{8}B and ^{7}Be is consistent with the measured one proton removal cross section and corresponds to an increase in the interaction radius of 4%. The existence of a substantial proton halo in ^{8}B is not supported by the present data.

PACS number(s): 25.60.+v, 25.70.Bc, 24.10.Eq

I. INTRODUCTION

Recently the nucleus ^{8}B has received much attention from both experimental and theoretical points of view. Its proton separation energy of only 137 keV and the location of its last proton in a p state with respect to the ^{7}Be core suggest that ^{8}B is a proton halo candidate [1]. Recent experiments provide contradictory information, pointing either toward a very large halo or to a vanishing one. In a recent experiment, Minamisono *et al.* [2] found an electric quadrupole moment much larger than a shell model prediction, which led them to claim the existence of a proton halo. However, measurements of interaction cross sections by Tanihata *et al.* [3] show no spectacular enhancement when compared to adjacent nuclei. A $(0+2)\hbar\omega$ shell model calculation by Nakada and Otsuka [4] suggests that the quadrupole momentum of ^{8}B can be explained without reference to a proton halo. Also the generator coordinate model (GCM) calculation of Descouvemont and Baye [5] shows no clear indication of a proton halo, while the resonating group model (RGM) multiconfiguration-multicluster calculation of Csótó [6] indicates a proton skin of 0.5 fm. It has been demonstrated that the behavior of the proton density distribution in ^{8}B at large distances may be important for the high energy component of the solar neutrino flux [1,7].

It should be noted that different experiments may probe the wave function of the proton interacting with the ^{7}Be core at different distances. The angular distributions of elastic scattering can, in principle, provide information on the density distributions and the corresponding optical potentials.

In this paper we present the results of the measurements of ^{7}Be,^{8}B+^{12}C quasielastic scattering at 40 MeV/nucleon. The scattering of ^{12}C+^{12}C at 20 MeV/nucleon was also measured in order to verify the method of extracting angular distributions from the experimental data.

The paper is organized as follows. The experimental method and data are presented in Sec. II. Section III reports the results of coupled-channels (CC) calculations, while Sec. IV deals with a detailed analysis of the reaction cross sections. In Sec. V the interpretation of the data is presented in semiclassical terms. The conclusions are summarized in Sec. VI.

II. EXPERIMENTAL METHOD

Secondary beams of ^{8}B and ^{7}Be, with a mean energy of 40 MeV/nucleon, were produced by fragmentation of a 60 MeV/nucleon ^{13}C beam on a 2 mm thick ^{9}Be target. The fragmentation products were subsequently separated using the doubly-achromatic spectrometer LISE3 [8]. The purity of the secondary beams was enhanced by the use of a 1120 μm thick aluminum wedge located at the first dispersive plane of LISE3 and by means of a Wien filter placed at the end of the spectrometer.

The mean intensity of the ^{8}B beam was 700 pps. The purity of the ^{8}B secondary beam was better than 99.2%. The momentum acceptance of the spectrometer in this case was limited to 1.1%. The ^{7}Be secondary beam had an intensity of 1000 pps, a momentum acceptance of 0.33%, and a purity of 98.4%. Finally, a ^{12}C beam of 2200 pps, of a purity of 99.9% and a momentum acceptance of 0.33%, was produced with the same ^{13}C primary

beam to test and measure the efficiency of the experimental setup in a wide range of angles. The diameter of the beam spot on the secondary target was in all three cases about 7 mm FWHM (full width at half maximum).

The experimental setup, shown in Fig. 1, was considerably improved compared to an earlier experiment performed with a ^{11}Li beam [9]. It consisted of two position sensitive (x, y) parallel-plate avalanche counters (PPAC) separated by $\sim$ 1 m. The second PPAC was placed 42 mm away from the secondary target which consisted of 18.5 mg/cm^2 of carbon. The position resolution of the PPAC's was 1.5 mm FWHM, which thus provided a measurement of the angle of secondary beam with a resolution better than 0.15°. Both PPAC's also provided start signals for time-of-flight (TOF) measurements with respect to the radiofrequency of the cyclotron.

The scattered particles were detected by an assembly of three silicon strip detectors ($E1, E2, E3$) with thicknesses of 150 μm, 500 μm, and 4500 μm, respectively. The $E1$ detector consisted of 32 circular strips of width 0.77 mm with a central hole of 15 mm diameter for the passage of the unscattered beam. The external diameter of the detector was 68 mm. The $E2$ detector comprised 32 radial strips with the same inner and outer diameters. The $E3$ detector was composed of four radial sectors and served as a stopping detector. The first two detectors also provided information on the energy loss which, in combination with the residual energy provided by the third detector, was used for particle identification. The overall energy resolution (4%) was not, however, sufficient to fully distinguish between elastic and inelastic scattering, hence the reference to quasielastic scattering. In order to increase the range of measured angles, the assembly of $E1$, $E2$, and $E3$ detectors was placed during the experiment at two different distances with respect to the target: 133 mm and 328 mm. The two settings had a wide angular overlap so that the extracted angular distributions could be compared with each other.

Downstream of the above assembly (see Fig. 1), a telescope consisting of 11 silicon detectors was used to monitor the secondary beam intensity and to measure the excitation function of the ^{8}B$\rightarrow^7$ Be $+ p$ breakup on silicon. The results of this measurement will be presented in detail in a forthcoming publication. The measurement of energy losses in different detectors of the telescope allowed us to separate and count also the ^{7}Be nuclei coming from the breakup of ^{8}B on a carbon target at 40 MeV/nucleon, giving a direct estimation of a breakup cross section.

Control measurements without the secondary target were performed in order to determine the contribution of background events coming from beam scattering on materials other than the target. The contribution was found to be less than 2%. A minimum deflection of 2° in the center-of-mass (c.m.) system (larger than the angular resolution by more than 3σ) was imposed in order to eliminate most of primary beam particles.

Extensive Monte Carlo simulations were performed in order to evaluate precisely the efficiency of the setup. The trajectories of the secondary beam particles, defined in the experiment on an event-by-event basis by the PPAC's, were used as input for the efficiency simulations. The trajectories of the particles after scattering on the target were then generated and efficiency was obtained as a function of the scattering angle, taking into account the geometry and all inactive areas in the detectors. It was verified that the efficiency depends only on geometrical structure of the system and not on the angular distribution used to generate the scattering angles. The calculated efficiency was then used for the determination of the experimental angular distributions. The finite spatial resolution of the PPAC's and of the strip detectors, as well as the multiple scattering and angular straggling in the target, were taken into account to obtain the final angular resolution for each angle.

The obtained data are shown in Fig. 2. A comparison of ^{12}C scattering data with the previously reported pure elastic scattering data measured by Bohlen *et al.*

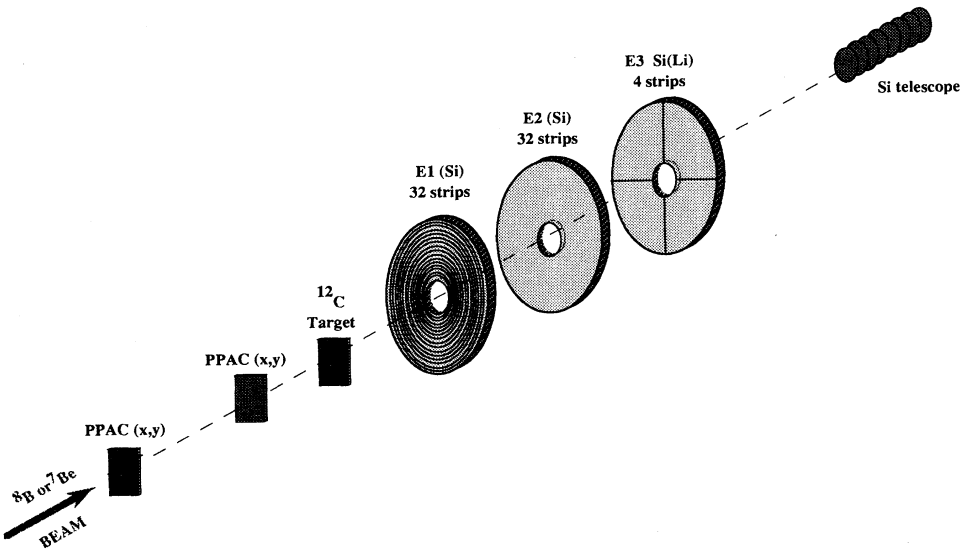

FIG. 1. Schematic diagram of the experimental setup.

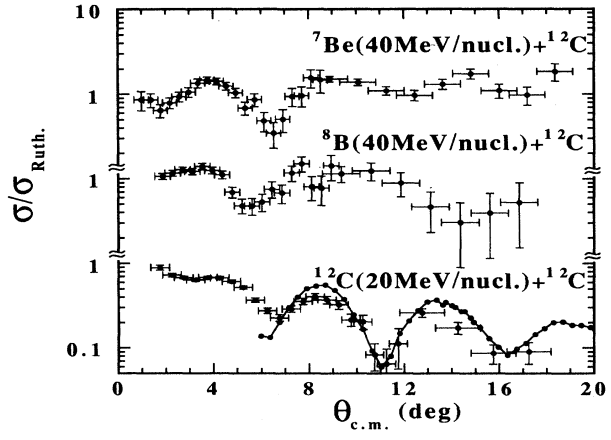

FIG. 2. Quasielastic scattering data obtained in the present work. The vertical error bars are statistical only, the horizontal ones were estimated by Monte Carlo simulation. The dots connected by a solid line indicate the ^{12}C+^{12}C elastic scattering data measured by Bohlen *et al.* [10].

[10] shows good agreement, thus confirming the data reduction technique used in the present study. It may be noted that in the present experiment it was possible to measure elastic scattering down to 2° (c.m.).

III. QUASIELASTIC SCATTERING

In the following, the quasielastic data obtained in this work are interpreted in terms of the distorted-wave Born approximation (DWBA) and coupled-channels (CC) approximations. Due to the restricted angular range and the considerable mixing of inelastic scattering, a direct fit to the data is difficult. We have therefore performed a comparison with a semimicroscopic prediction for elastic and inelastic cross sections.

A. Optical potentials and density calculations

The double folding model associated with the effective interaction of Jeukenne, Lejeune, and Mahaux (JLM) [11] was chosen to construct the necessary elastic optical potentials and the form factors for inelastic scattering. In Ref. [11], a complex density, and energy dependent interaction was derived in such a way that the entire nucleon-nucleon potential can be obtained with the Hartree term only. The density dependence is treated in the local density approximation. The results for volume integrals and mean radii of the predicted optical potentials are greatly improved by introducing a finite range smearing function. The imaginary part has a correct behavior near the Fermi surface and includes effective mass correction.

Starting from JLM effective interaction, the heavy ion optical potential $U(R)$ can be constructed in the double folding model in the following way:

$$U(R) = N_V V(R) + iN_W W(R) \ ,$$

where

$$V(R) = \int d\mathbf{r}_1 d\mathbf{r}_2 \rho_1(r_1)\rho_2(r_2)\mathrm{Re}v_{\mathrm{eff}}(|\mathbf{R}+\mathbf{r}_1-\mathbf{r}_2|,\rho,E) \ ,$$

$$W(R) = \int d\mathbf{r}_1 d\mathbf{r}_2 \rho_1(r_1)\rho_2(r_2)\mathrm{Im}v_{\mathrm{eff}}(|\mathbf{R}+\mathbf{r}_1-\mathbf{r}_2|,\rho,E) \ .$$

In the above formulas, $\mathbf{R}, \mathbf{r}_1, \mathbf{r}_2$ are the usual double folding variables and $\rho_{1,2}$ are the one-body densities. The functional form of the real and imaginary parts of the effective interaction are taken from [11] and evaluated at $E = E_{\mathrm{lab}}/A_{\mathrm{proj}}$. Only the isoscalar components have been retained. For consistency, the Coulomb component of the optical model has been calculated in the double folding model. Coulomb corrections arising from nonlocality and energy dependence of the effective interaction were neglected because they are only important near the Coulomb barrier.

In extrapolating to heavy ions, the main difficulty arises from the ambiguity in the definition of density ρ in the overlap region. Since the JLM interaction is not defined for densities larger than the equilibrium density of nuclear matter, we have chosen the approximation

$$\rho(r_1,r_2) = [\rho_1(r_1)\rho_2(r_2)]^{1/2} \ , \qquad (1)$$

which underestimates the density for strong overlaps but does not give rise to unphysical situations, as does the usual approximation: $\rho(r_1,r_2) = \rho_1(r_1) + \rho_2(r_2)$. The bare folding optical potential contains only two parameters: the normalization constants N_V and N_W for the real and imaginary parts, respectively. This normalization is necessary in order to compensate for the underestimation of the density in the overlap region and for high order effects in the optical potential.

The diagonal part of the one-body densities for ^{7}Be and ^{8}B in the **r** space have been obtained in a multiconfigurational shell-model (SM) calculation. The occupation probabilities were obtained by diagonalization of the Warburton-Brown interaction [12] in the first four major shells using the OXBASH code [13]. The spurious center-of-mass motion was removed by the usual method [14], by adding the center-of-mass Hamiltonian to the interaction. The first four major shells provide a completely nonspurious shell-model basis when $2\hbar\omega$ configurations are included. The residual interaction used in the shell-model procedure does not fix the single particle wave functions (SPWF). We have chosen the Hartree-Fock (HF) SPWF as a basis, which seems to be more adequate to describe the nuclear surface. The Skyrme III force (SkIII) [15] and the occupation probabilities from the SM calculation were used as inputs to the HF calculation. For consistencey, the ^{12}C one-body density was obtained in a standard HF SkIII calculation.

As can be seen from Table I, the SM calculations predict comparable proton skins for ^{7}Be and ^{8}B nuclei, the skin being defined by the difference between root mean square (RMS) radii of the proton and neutron distributions. Table I includes for comparison the RMS radii for

TABLE I. RMS radii for proton (p), neutron (n), and matter (m) density distributions obtained with the shell model (SM) and a standard Hartree-Fock calculation (SkIII). The values obtained by Tanihata *et al.* [3] from interaction cross sections are also included (HO).

	$\langle r_p^2\rangle^{1/2}$	$\langle r_n^2\rangle^{1/2}$	$\langle r_m^2\rangle^{1/2}$	$\langle r_p^2\rangle^{1/2}$-$\langle r_n^2\rangle^{1/2}$	Density
	(fm)	(fm)	(fm)	(fm)	
	2.337	2.108	2.242	0.229	SM
^{7}Be	2.148	1.972	2.075	0.176	SkIII
	2.36±0.02	2.25±0.02	2.31±0.02	0.11±0.03	HO
	2.400	2.068	2.281	0.332	SM
^{8}B	2.317	2.010	2.207	0.307	SkIII
	2.45±0.05	2.27±0.04	2.38±0.04	0.18±0.06	HO
^{12}C	2.423	2.398	2.410	0.020	SkIII

HF densities calculated with the SkIII effective interaction. These are systematically smaller than the corresponding SM values, although the proton skin is comparable. This highlights the importance of configuration mixing and reflects the uncertainty in the Skyrme-type parametrization, which is adjusted to properties of nuclei near the stability line. The RMS radii of proton distributions predicted by the present SM calculations are nearly identical with the corresponding values extracted by Tanihata *et al.* [3] from interaction cross sections, using harmonic oscillator (HO) wave functions, while the RMS radii for the neutron distributions are smaller by $\sim$ 0.15 fm. Consequently, the SM proton skin is two times larger than the HO value. Other microscopic calculations [4–6] predict even larger proton skins. Therefore, the existence of a proton skin in proton rich nuclei is quite natural, provided the wave functions have the correct asymptotic behavior [4,5]. These very diffuse densities may induce an increase of refraction effects in elastic scattering for both nuclei. However, we expect that the larger absorption for ^{8}B (due to the smaller threshold for breakup) will produce an additional damping of the ^{8}B elastic cross section.

B. ^{12}C scattering

For the ^{12}C+^{12}C case, the interaction was fixed by fitting the original data of Bohlen *et al.* in a standard CC calculation. The ^{12}C nucleus was treated as a rigid rotor and couplings involving both excitation and deexcitation between ground state (0^+) and first excited state (2^+, 4.44 MeV) were used. The $B(E2\uparrow)$ value was taken from the compilation of Raman *et al.* [16] and the same deformation length was used for all components of the optical potential. With the normalization constants $N_V = 0.56$ and $N_W = 0.84$ the agreement with the data of Bohlen *et al.* is good, especially in the diffractive region (Fig. 3). The above results demonstrate that our folding potentials can be safely used to describe both elastic and inelastic scattering and should diminish any ambiguities in the interpretation of ^{7}Be and ^{8}B quasielastic scattering.

The above calculation is also compared with our experimental data on ^{12}C+^{12}C quasielastic scattering (Fig. 4). The excitation of the 3^- state was calculated using the DWBA and vibrational model, with a deformation length δ_3 taken from Ref. [17]. The inelastic scattering and finite angular resolution account well for the filling of the minima. The satisfactory agreement obtained with the ^{12}C+^{12}C data provides confidence in the interpretation of the data.

C. ^{7}Be and ^{8}B scattering

The same type of calculation has been performed for ^{7}Be and ^{8}B quasielastic scattering. In these cases the normalization constants N_V and N_W were obtained by fitting the pure elastic scattering of ^{6}Li+^{12}C at 26 MeV/nucleon, 35 MeV/nucleon, and 53 MeV/nucleon [18–20]. All spurious solutions were eliminated by retaining only the smooth energy dependence of the normalization constants. Fits, as good as in the ^{12}C+^{12}C case, were obtained in the full angular range, including the so-called rainbow region, which shows that our interaction has a correct behavior well inside the strong absorption radius. The interpolated values for an energy of 40 MeV/nucleon are $N_V = 0.65$ and $N_W = 0.80$. The

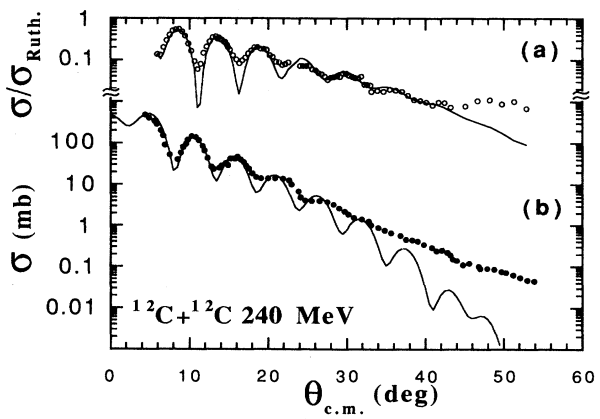

FIG. 3. CC calculation of (a) elastic and (b) inelastic (2^+) scattering (solid lines) compared with the experimental data of Bohlen *et al.* [10] (points).

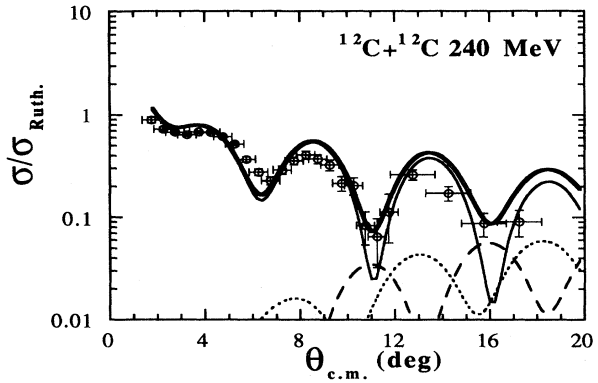

FIG. 4. CC calculation of the elastic (thin solid line) and the inelastic (2^+) (dashed line) scattering. The contribution of the (3^-) state of ^{12}C is calculated in DWBA (dotted line). The incoherent sum of elastic and both inelastic channels (thick solid line) is compared with experimental data (points). The experimental angular resolution was taken into account in the calculations.

large reduction of the real part arises mainly from the underestimation of the density effects by the approximation (1). By taking the normalization constants from ^{6}Li+^{12}C scattering, a large part of the repulsive dynamical polarization potential (DPP) arising from the strong coupling to the breakup channel is already included in our potentials. This fact explains the increased value of the renormalization of the real part with respect to the ^{12}C+^{12}C case, where the breakup effects are of less importance. As can be seen from Fig. 5(a) the agreement with the quasielastic data is good for ^{7}Be—both the magnitude and the oscillations are correctly reproduced. The excitation of the 2^+ state in ^{12}C accounts to a large extent for the filling of first deep minimum at 6.5° and the contribution becomes comparable with the elastic scattering at angles larger than 10°. The excitation of the 3^- state, although much smaller in amplitude, gives a non-negligible contribution at large angles. We have also verified that the first excited state in ^{7}Be gives a negligibly small contribution to the angular distribution.

The same type of CC calculation was performed for ^{8}B quasielastic scattering and compared with the data in Fig. 5(b). The agreement with the data is worse than in the ^{7}Be case. The structures shown by the data are less pronounced. The filling of the minima cannot be entirely explained by inelastic contribution from the target excitation. One might suspect an additional contribution from projectile excitation. In order to check this hypothesis, a separate CC calculation has been undertaken to evaluate the contribution of a quasibound (1^+, 0.77 MeV) level placed just above the ^{7}Be+p threshold. The reduced transition probability was taken from the GCM estimation of Descouvemont and Baye [5]. The inelastic cross section was added incoherently to the results of the preceding calculation. As can be seen in Fig. 6, projectile excitation does not significantly change the results.

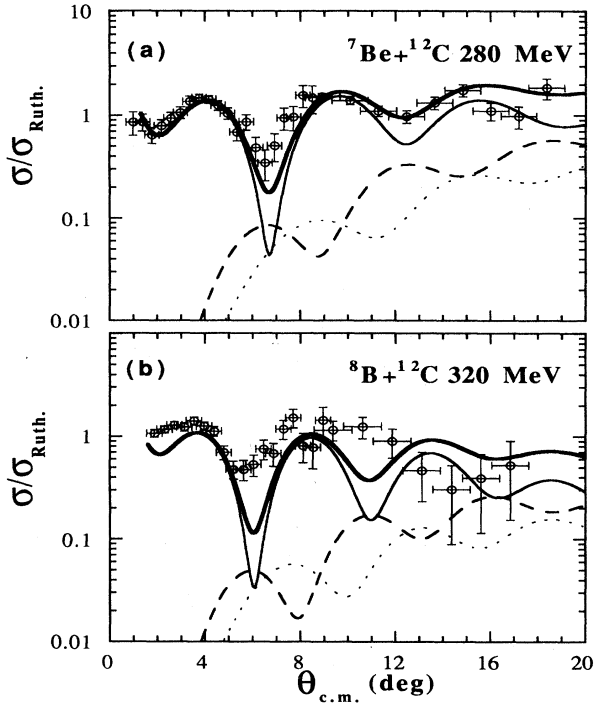

FIG. 5. CC calculation of elastic (thin solid line) and inelastic (2^+) (dashed line) scattering. The contribution of the (3^-) state in ^{12}C is calculated in DWBA (dotted line). The incoherent sum of elastic and both inelastic channels (thick solid line) is compared with experimental data (points). The experimental angular resolution was taken into account in the calculations.

The calculation presented in Fig. 6 shows a discrepancy in the magnitude of cross section at angles corresponding to diffraction minima. Tests with different optical potentials, e.g., a double folding potential with the standard $M3Y$ effective interaction as well as a simple Woods-Saxon one [29], resulted in even more pro-

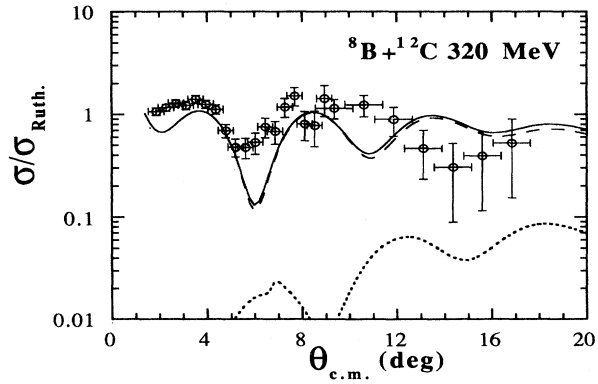

FIG. 6. CC estimation of the contribution of the excited state (1^+) in ^{8}B (dotted line). The dashed line represents the result of the preceding calculation [Fig. 5(b)]. The solid line is the incoherent sum of all channels.

nounced minima comparing to the experimental data. These facts suggest that the data for the loosely bound nucleus ^{8}B cannot be satisfactorily described by optical model amplitudes. Similar discrepancies were found for elastic scattering of another loosely bound nucleus ^{11}Li on silicon [9] and carbon [21], where the cross section at small angles is underestimated by the optical model.

IV. REACTION CROSS SECTION

Further information can be obtained from reaction cross sections (see Table II). We compare our results denoted by JLM with the phenomenological formula of Kox [22] using the isospin component suggested by Zahar *et al.* [23]. The individual radii were calculated in two ways. In the first, we have used the liquid drop model parametrization, also used by Shen *et al.* [24] in a similar calculation. In a subsequent calculation, the mean square radii from the present SM calculations were used for ^{7}Be and ^{8}B together with the SkIII value for ^{12}C. The JLM folding model predicts an increase in the reaction cross section of 78 mb for ^{8}B. An experimental estimation of breakup on the ^{12}C target, extracted from the independent measurement using the silicon telescope, gives $\sigma_{-p} = 80 \pm 15$ mb. This value is consistent with the result of a Glauber-type calculation using the two-body wave functions of Riisager and Jensen [1] and compares well with the breakup cross section (σ_{-p}) of 60 ± 5 mb obtained by Corre [25] for the reaction ^{8}B+^{28}Si$\rightarrow^7$Be+p+^{28}Si at the same energy. This suggests an approximate factorization of the proton-core wave function and shows that a Glauber-type relation,

$$\sigma_{-p} = \sigma_R(^8\mathrm{B}) - \sigma_R(^7\mathrm{Be}) \qquad (2)$$

is also valid for the proton breakup of ^{8}B. We further checked this hypothesis by calculating the individual cross sections appearing in (2), using the optical limit of the Glauber theory:

$$\sigma_R = 2\pi \int_0^\infty b\, db[1 - T(b)] ,$$

where the transparency function $T(b)$ is given by [28]

$$T(b) = e^{-\chi(b)} ,$$

$$\chi^{(b)} = \sum_{\alpha,\beta=p,n} \sigma_{\alpha\beta}^{\mathrm{NN}} \int d\mathbf{b}_1 d\mathbf{b}_2 \rho_{1\alpha}(b_1)\rho_{2\beta}(b_2) \times f(\mathbf{b} + \mathbf{b}_1 - \mathbf{b}_2) ,$$

and where $\sigma_{\alpha\beta}^{\mathrm{NN}}$ are the effective NN (nucleon-nucleon) total cross sections and $\rho_{1(2)\alpha(\beta)}$ are the density profiles obtained by projecting the individual densities onto the impact parameter plane. As suggested by Bertsch *et al.* [28], the smearing function f is taken as a normalized Gaussian with a range of 0.9 fm. The above formula does not include corrections for Fermi motion, Pauli blocking, and deflection of the trajectories in the nuclear field. However, there is an approximate cancellation between these effects and the above formula predicts relative ecross sections with good accuracy. The results are given in Table II in which the experimental interaction cross section obtained by Tanihata *et al.* [3] at 790 MeV/nucleon is included for completeness. The difference in the reaction cross section (about 8%) corresponds to an increase of the interaction radius of 4%, compatible with an $A^{1/3}$ dependence. Tanihata *et al.* [3] found a 3% increase at 790 MeV/nucleon. The existence, therefore, of a substantial proton halo in ^{8}B is not supported by the present data.

The rather small increase of the interaction radius found here could be understood in terms of an effective separation energy [26],

$$S_{\mathrm{eff}} = S_p + B_c , \qquad (3)$$

where B_c is the Coulomb barrier and $S_p = 0.137$ MeV. For ^{8}B, the Coulomb barrier contributes about 2 MeV to the effective separation energy. Consequently the Coulomb barrier is largely responsible for the confining of the last bound proton and thus inhibiting the development of a distribution of large radial extent.

TABLE II. Reaction cross sections (see text for details). Experimental interaction cross sections obtained by Tanihata *et al.* [3] at 790 MeV/nucleon are also included.

	Reaction cross section (mb)	
	^{7}Be+^{12}C	^{8}B+^{12}C
JLM[a]	1026	1104
Kox[b]	1037	1186
Kox[c]	1062	1179
Glauber[d]	1034	1111
Glauber[e]	1080	1130
Expt.[f]	738±9	784±14

[a]JLM folding model and SM densities.
[b]Kox formula as modified by Zahar *et al.* [23].
[c]The same as b but using SM radii from Table I.
[d]Glauber formula and SkIII densities.
[e]Glauber formula and SM densities.
[f]Reference [3].

V. SEMICLASSICAL ANALYSIS

It is interesting to compare the pair of nuclei ^{7}Be,^{8}B studied in the present paper and the pair ^{11}C,^{11}Li recently analyzed by Hussein and Satchler [27]. On the basis of semiclassical arguments, they found that for loosely bound nuclei like ^{11}Li, the increased extension of the one-body density (due to the halo) enhances the refractive power of the real optical potential. The corresponding enhancement of the elastic cross section is then compensated by the increased absorption due to the halo. Also, the strong coupling with the breakup channel gives rise to an additional damping of the elastic cross section through the long tail of the imaginary part of the induced dynamical polarization potential (DPP). The presumably repulsive real part of the DPP gives rise to smaller damping

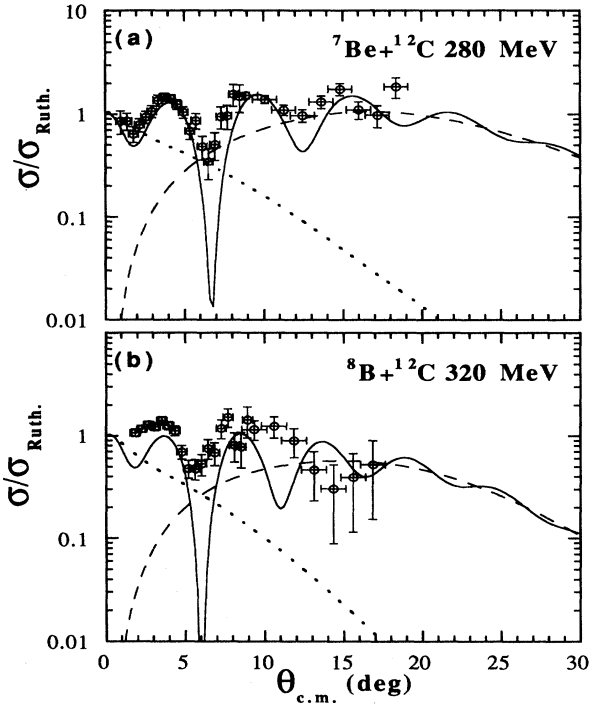

FIG. 7. Farside (dashed)-nearside (dotted) decomposition for elastic scattering of (a) ^{8}Be and (b) ^{8}B on ^{12}C. The solid lines correspond to the one channel elastic scattering. All curves are calculated with the JLM interaction.

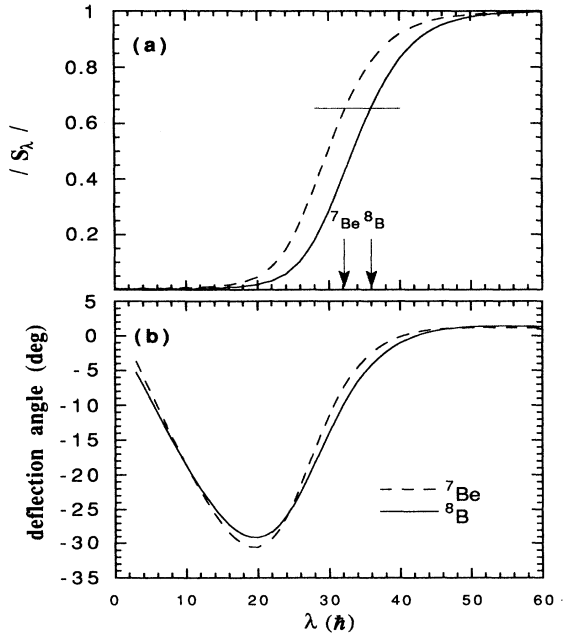

FIG. 8. (a) Optical model absorption profiles. The arrows indicate the conventional strong absorption angular momentum. (b) WKB deflection functions. The solid line corresponds to ^{8}B, the dashed one to ^{7}Be.

at large angles.

We have investigated such effects in the present data. A farside-nearside decomposition of the elastic cross seciton is presented in Fig. 7. Beyond the crossover angle, both cross sections are farside dominated, but the farside component decreases much faster for ^{8}B than for ^{7}Be at large angles. According to Hussein and Satchler [27], this effect may be attributed to an increased imaginary part of the complex angular momentum in the case of ^{8}B.

Additional information can be obtained from optical model absorption profiles [Fig. 8(a)] and the WKB deflection functions [Fig. 8(b)]. In both figures, the curves correspond to the bare JLM folding potential. The bright side of the deflection function is similar in these two cases, while the dark component is slightly more diffuse for ^{8}B. The rainbow angle $\theta_R \sim -30°$ corresponds to an angular momentum $\lambda_R \sim 20\hbar$. As can be seen from the absorption profiles, the rainbow effect in the cross section is removed by the strong absorption corresponding to trajectories with $\lambda < \lambda_R$. Beyond the crossover angle, the cross section is dominated by the $\lambda_>$ branch of the deflection function. Since $\lambda_>(^7\text{Be}) < \lambda_>(^8\text{B})$ the cross section for ^{8}B appears more damped than for ^{7}Be at these angles.

VI. SUMMARY

The quasielastic scattering of ^{7}Be and ^{8}B at 40 MeV/nucleon on ^{12}C target has been measured. The experimental method and data reduction techniques were carefully tested by comparing our ^{12}C+^{12}C (20 MeV/nucleon) measurement with the existing data of Bohlen *et al.* [10]. Extensive Monte Carlo simulations were performed to extract the geometrical efficiency of the setup and to estimate the experimental uncertainties. Shell model one-body densities and the effective interaction of Jeukenne, Lejeune, and Mahaux [11] were used to generate the elastic optical potentials and the form factors for inelastic scattering. Our SM calculation for the one-body densities predicts a significant proton skin for both ^{7}Be and ^{8}B nuclei. The normalization constants of the effective interaction extrapolated from ^{6}Li+^{12}C data at similar energy and coupled-channels (CC) calculations account well for the quasielastic scattering data of ^{7}Be. However, the CC calculation for ^{8}B does not satisfactorily reproduce the quasielastic scattering data. As in the case of ^{11}Li it is difficult to reproduce the small angle cross section with a simple optical model. This feature reflects probably the loosely bound nature of both nuclei. Good agreement was obtained, however, between our measured one proton removal cross section ($\sigma_{-p} \sim 80$ mb) and the difference in the total reaction cross section for ^{8}B and ^{7}Be. The experimental one proton removal cross section agrees well with a Glauber-type calculation. These results do not support the existence of a substantial proton halo in ^{8}B.

A semiclassical analysis revealed a number of similar-

ities for ^{8}B with ^{11}Li resulting from a combined effect of the low threshold for breakup and of proton or neutron skin. The stronger Coulomb interaction in ^{8}B confines the proton wave function in the nuclear interior and inhibits the development of a proton halo. The folding potentials generated by the JLM microscopic effective interaction (which has a correct mass and energy dependence) are much stronger for ^{8}B than for ^{7}Be in both real and imaginary parts. The increased refraction is masked by the stronger absorptive part of the potential and the resulting ^{8}B elastic cross section appears much damped at large angles compared to that for the ^{7}Be.

ACKNOWLEDGMENTS

We are much indebted to M. Horoi for providing us with the SM occupation numbers and to N. Orr for valuable comments and discussions. We thank A. Nadasen, H. Bohlen, and H. Rebel for providing the elastic cross section data. Technical support of R. Hue and F. Geoffroy is also acknowledged. One of the authors (A.K.) acknowledges financial support from the Polish State Committee for Scientific Research under Grant No. 2P302 215 04.

[1] K. Riisager and A. S. Jensen, Phys. Lett. B **301**, 6 (1993).
[2] T. Minamisono *et al.*, Phys. Rev. Lett. **69**, 2058 (1992).
[3] I. Tanihata, H. Hamagaki, O. Hashimoto, Y. Shida, N. Yoshikawa, K. Sugimoto, O. Yamakawa, T. Kobayashi, and N. Takahashi, Phys. Rev. Lett. **55**, 2676 (1985); I. Tanihata, T. Kobayashi, O. Yamakawa, T. Shimoura, K. Ekuni, K. Sugimoto, N. Takahashi, T. Shimoda, and H. Sato, Phys. Lett. B **206**, 592 (1988).
[4] H. Nakada and T. Otsuka, Phys. Rev. C **49**, 886 (1994).
[5] P. Descouvemont and D. Baye, Nucl. Phys. **A567**, 341 (1994); D. Baye, P. Descouvemont, and N. K. Timofeyuk, *ibid.* **A577**, 624 (1994).
[6] A. Csótó, Phys. Lett. B **315**, 24 (1993).
[7] J. N. Bahcall, W. F. Huebner, S. H. Lubow, P. D. Parker, and R. K. Ulrich, Rev. Mod. Phys. **54**, 767 (1982).
[8] R. Anne and A. C. Mueller, Nucl. Instrum. Methods B **70**, 276 (1992).
[9] M. Lewitowicz *et al.*, Nucl. Phys. **A562**, 301 (1993).
[10] H. G. Bohlen *et al.*, Z. Phys. A **322**, 241 (1985).
[11] J.-P. Jeukenne, A. Lejeune, and C. Mahaux, Phys. Rev. C **16**, 80 (1977).
[12] E. K. Warburton and B. A. Brown, Phys. Rev. C **46**, 923 (1992).
[13] B. A. Brown *et al.*, MSUNSCL Report No. 524 (1988).
[14] D. H. Gloeckner and R. D. Lawson, Phys. Lett. **53B** , 313 (1974).
[15] M. Beiner, H. Flocard, Nguyen van Giai, and P. Quentin, Nucl. Phys. **A238**, 28 (1975).
[16] S. Raman, C. W. Nestor, Jr., S. Kahane and K. H. Bhatt, At. Data Nucl. Data Tables **42**, 1 (1989).
[17] R. H. Spear, At. Data Nucl. Data Tables **42**, 55 (1989).
[18] J. Cook, H. J. Gils, H. Rebel, Z. Majka, and H. Klewe-Nebenius, KfK Report No. 3233 (1981).
[19] A. Nadasen *et al.*, Phys. Rev. C **37**, 132 (1988).
[20] A. Nadasen *et al.*, Phys. Rev. C **47**, 674 (1993).
[21] J. J. Kolata *et al.*, Phys. Rev. Lett. **69**, 2631 (1992).
[22] S. Kox *et al.*, Phys. Rev. C **35**, 1678 (1987).
[23] M. Zahar *et al.*, Phys. Rev. C **49**, 1540 (1994).
[24] Shen Wen-qing, Wang Bing, Feng Jun, Zhan Wen-long, Zhu Yong-tai, and Feng En-pu, Nucl. Phys. **A491**, 130 (1989).
[25] J.-M. Corre, Ph.D. thesis, University of Caen, 1994.
[26] M. Lassaut and R. J. Lombard, in *Proceedings of the 6th International Conference on Nuclei Far from Stability and the 9th International Conference on Atomic Masses and Fundamental Constants, Bernkastel-Kues, 1992*, edited by R. Neugart and A. Wöhr (IOP, Bristol, 1993).
[27] M. S. Hussein and G. R. Satchler, Nucl. Phys. **A567**, 165 (1994).
[28] G. F. Bertsch, B. A. Brown, and H. Sagawa, Phys. Rev. C **39**, 1154 (1989).
[29] M. Lewitowicz *et al.*, in *Proceedings of the 7th International Conference on Nuclear Reaction Mechanisms, Varenna, 1994*, edited by E. Gadioli (Universita degli Studi di Milano, Ricerca Scientifica ed Educazione Permanente, Milano, 1994), p. 528.